DOI: 10.1002/ejic.200900138

Simultaneous Gas-Phase Loading of MOF-5 with Two Metal Precursors: towards Bimetallics@MOF

Felicitas Schröder,[a] Sebastian Henke,[a] Xiaoning Zhang,[a] and Roland A. Fischer*[a]

Keywords: Nanoparticles / Metal-organic frameworks / Gas-phase reactions

Simultaneous gas-phase loading of $[Zn_4O(bdc)_3]$ (bdc = 1,4-benzenedicarboxylate; MOF-5) with combinations of two different MOCVD precursors such as $[Fe(\eta^6\text{-toluene})(\eta^4\text{-}C_4H_6)]$/$[CpPtMe_3]$, $[CpPd(\eta^3\text{-}C_3H_5)]$/$[CpPtMe_3]$ and $[Ru(cod)(cot)]$/$[Pt(cod)Me_2]$ was followed by solid state ^{13}C MAS NMR spectroscopy, elemental analysis and X-ray powder diffraction (PXRD). Different amounts of precursors were applied for the loading experiments. It was found that defined molar ratios of the adsorbed precursors inside MOF-5 can be achieved when the loading is below the saturation level of MOF-5 for adsorption of the individual precursors. The co-hydrogenolysis of the loaded material $[Ru(cod)(cot)]$/$[Pt(cod)Me_2]$@MOF-5 was selected as a representative example to study the possibility of obtaining bimetallic PtRu nanoparticles hosted inside the MOF support. The quantitative co-hydrogenolysis of the adsorbed metal precursors led to formation of alloyed metal nanoparticles as revealed by PXRD, transmission electron microscopy (TEM) and selected area electron diffraction. However, the bdc linkers of the MOF-5 host material were partially hydrogenated which caused a severe distortion of the MOF-5 matrix, loss of long range crystalline order and reduction of the BET surface area down to 380 $m^2 g^{-1}$.

Introduction

Metal-organic frameworks (MOFs) or porous coordination polymers (PCPs) have been shown to be suitable as zeolite-like host matrices for the imbedding or supporting of functional nanoparticles.[1] In particular, $[Zn_4O(bdc)_3]$ (bdc = 1,4-benzenedicarboxylate; MOF-5) and $[Zn_4O(btb)_3]$ (btb = 1,3,5-benzentribenzoate) were selected as the first test cases for the solvent-free gas phase loading with metal or metal oxide precursor compounds, followed by conversion of the adsorbed precursors into the desired metal or metal oxide particles (ideally) inside the host matrix. The obtained materials are denoted as "Metals@MOF" and "Metaloxide@MOF".[1] Thus, MOFs emerge as a new family of chemically and structurally the most variable porous matrices for stabilisation of nanoparticles. Still, only few groups[1] have followed these ideas and we wish to highlight the recent work of Haruta et al. who reported quite interesting catalytic properties of supported Au/MOF catalysts for the liquid phase oxidation of alcohols.[2]

So far, all reports on Metals@MOFs or similar PCP-based nanocomposite containing nanodispersed metal particles deal with single metals. However, the simultaneous loading with two metal precursor components and their co-decomposition to yield alloy particles appears to be a straight forward extension of this research. Among the fascinating properties of bimetallic nanoparticles, only a few will be addressed here. For instance, the fully ordered fct (face-centred tetragonal) structured FePt alloy exhibits an anisotropy constant K that is among the highest of all known hard magnetic materials.[3] Therefore bimetallic superparamagnetic FePt nanoparticles are expected to become the density limit for magnetic memory devices.[4,5] In catalytic applications, the addition of a second metal can improve the activity and/or selectivity of metallic catalysts.[6,7] For instance, the addition of Pd to Au catalysts significantly enhances the catalytic performance in H_2O_2 synthesis. For instance, the H_2O_2 production rate of a bimetallic Pd/Au catalyst exceeds the production rates of pure Pd or Au catalysts.[8] In the hydrogenation reaction of cinnamaldehyde to cinnamyl alcohol, PtRu catalysts showed a notably improved selectivity which was up to two times higher than for the corresponding monometallic catalysts.[9] Furthermore, PtRu nanoparticles are so far the most promising anode catalysts in direct methanol fuel cells since PtRu nanoparticles exhibit an excellent tolerance towards the poisoning CO formed during methanol oxidation.[10]

To achieve the formation of bimetallic nanoparticles in MOF-5 materials by the co-hydrogenolysis of two *all-hydrocarbon* metal precursors under hydrogen pressure, we adopted the concepts developed by the group of B. Chaudret for the synthesis of colloidal alloy nanoparticles in non-

[a] Anorganische Chemie II – Organometallics & Materials, Ruhr-Universität Bochum,
Universitätsstrasse 150, 44780 Bochum, Germany
Fax: +49-234-32-14171
E-mail: Roland.Fischer@rub.de

Supporting information for this article is available on the WWW under http://dx.doi.org/10.1002/ejic.200900138.

aqueous solutions.[11] The crucial point in bimetallic nanoparticle synthesis in MOF materials as solid support matrices however, is the adjustment of a defined metal(1)/metal(2) molar ratio. In contrast to bimetallic colloid synthesis in solution, the stoichiometry of the precursor compounds adsorbed *inside* the MOFs is difficult to control. Solution impregnation (incipient wetness method) of MOFs for metal loading has been shown to be limited to low loadings of a few wt.-%.[1c,1g] Thus, just using different molar concentrations of the two precursor components in solution is possibly not a very versatile option for MOF loading. Gas-phase loading with two different precursors on the other hand may be complicated by different transport, adsorption and reactive properties of the chosen precursors.

In this work, the simultaneous gas-phase loading of MOF-5 with the three precursor combinations [Fe(η^6-toluene)(η^4-C_4H_6)] (**A**)/[$CpPtMe_3$] (**B**), [CpPd(η^3-C_3H_5)] (**C**)/[$CpPtMe_3$] and [Ru(cod)(cot)] (**D**)/[Pt(cod)Me_2] (**E**) was investigated (see Scheme 1). As in our previous reports on Pd, Cu, Au and Ru nanoparticle synthesis inside MOF-5,[1a,1d,1e,1g] the gas-phase loading experiments were also carried out under static conditions at reduced pressure ($< 10^{-1}$ mbar). Different precursor amounts and molar ratios were applied for the simultaneous loading experiments, followed by elemental/AAS analysis (atomic absorption spectroscopy), ^{13}C MAS NMR (magic angle spinning nuclear magnetic resonance) and PXRD (powder X-ray diffraction) structural investigations of the obtained composites. Finally, the co-decomposition of [Ru(cod)(cot)] (**D**) and [Pt(cod)Me_2] (**E**) embedded in MOF-5 was also investigated, followed by ^{13}C MAS NMR, PXRD and TEM (transmission electron microscopy) studies in order to examine the nature of the obtained metal nanoparticles.

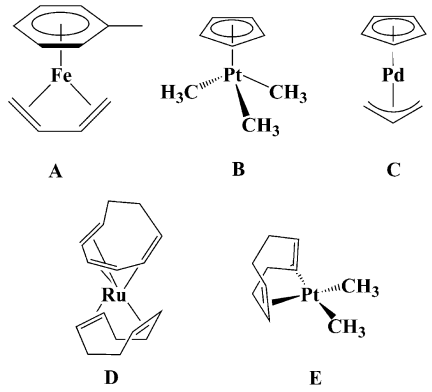

Scheme 1. Precursors **A**–**E** selected for absorption by MOF-5.

Results and Discussion

1. Simultaneous Loading of MOF-5 with two Precursors for Different Metals

In order to gain an initial understanding of the gas-phase loading of MOF-5 with two different metal precursors, we chose the precursor combinations shown in Table 1 and the loading procedure was carried out in a similar way to that described before for loading with single precursors,[1b] under static conditions at room temperature (20–25 °C) and pressures of 0.01–0.1 mbar depending on the vapour pressure of the precursors (which is in the range of 0.03 to 0.06 mbar at 23 °C).[12,13] The resultant products with the precursors adsorbed inside the cavities of MOF-5 were characterised by ^{13}C MAS NMR spectroscopy, PXRD and elemental/AAS analyses. The chosen precursors exhibit all-hydrocarbon coordination spheres which are quite similar in chemical nature, size and shape.[1b] Note that the loading capacity of MOF-5 for ferrocene, as the prototype for this class of compounds, is about 56 molecules per elementary cell or 7 mol of ferrocene per MOF-5 formula unit.[14] This appears to be the thermodynamic loading limit for ferrocene under static conditions of 120 °C and 3.5 mbar (vapour pressure of ferrocene). A corresponding saturated loading with the related organometallic compounds of Scheme 1 is difficult to achieve because of their comparably high thermal instability. However, a single loading of about 3–4 mol of **A**–**E** per MOF-5 formula unit was obtained at moderately elevated temperatures of 70–80 °C.[1b,1d] This loading level could also be nicely reproduced at the lower temperature of 25 °C in the cases **A/B**, **B/C** and **D/E** as deduced from the elemental analyses of the composites (Table 1). In the case of **D/E**, a quantitative adsorption in a 1:1 (± 0.1) molar ratio was achieved reproducibly − no organometallic compounds were left in the vials. In the other cases **A/B** and **B/C**, even higher amounts of precursor were chosen, however the total loading was not significantly higher. An excess of solid precursors **A**–**C** were left in the vials (mass balance ca. 95–99%). The variation of the molar ratio of **B** and **C** from 1:1 to 1:6 indicates a preferential adsorption of **C** over **B** (Table 1). The reasons for this observation are not yet apparent. Neither the vapour pressures nor the adsorption properties of **A**–**E** are likely to be that different. Note, that in *single* precursor loading experiments, **C** is favoured over **B** by adsorption of 4 vs. 3 mol per MOF-5 formula unit at higher temperatures (80 °C).[1b] More experiments at various precursor ratios, temperature/pressure ranges and at different time scales and are needed to clarify this issue and to distinguish between thermodynamic and kinetic factors. Nevertheless, the examples show that a controlled mixed loading (co-adsorption) is possible. The equimolar loading of example **D/E** is due to *quantitative adsorption* of both precursors which are apparently not that different in their adsorption properties (mass balance, yield 99%, see experimental part). Note, that the adsorption of **A**–**E** at MOF-5 is quite weak. Quantitative desorption takes place in dynamic vacuo at 25 °C/10^{-3} mbar over several hours.[1a,1b,1d]

The MAS-NMR spectroscopic characterisations of the composites **1**–**5** were in good agreement with what was expected from related previous data.[1a,1b,1d] Here, we would like to concentrate on the MAS-NMR spectroscopic properties of [Fe(η^6-toluene)(η^4-C_4H_6)]/[$CpPtMe_3$]@MOF-5 (**1**) and [Ru(cod)(cot)]/[Pt(cod)Me_2]@MOF-5 (**5**) (Figure 1, 2; Table 1). The MAS-NMR spectroscopic data of [CpPd(η^3-

Table 1. Numbering scheme of samples **1**–**5**. Molar ratios of the precursors **A/B**, **B/C** and **D/E** used for loading and the respective molar ratios and total moles of the adsorbed precursors per MOF-5 formula unit in the obtained composites. Note the adsorption limit of 4 mol precursor per MOF-5 formula unit for single precursor loadings at the same temperature/pressure conditions.[1b,1d]

Precursor combination	Molar ratio employed (precursor)	Molar ratio found (composite)	Total moles adsorbed of **A**–**E**
[Fe(η^6-toluene)(η^4-C_4H_6)] [$CpPtMe_3$] (**A/B**)	1:1	1.4:1 (**1**)	3.8
[$CpPd(\eta^3$-C_3H_5)] [$CpPtMe_3$] (**B/C**)	1:1	2.7:1 (**2**)	3.3
	3:1	4.1:1 (**3**)	3.4
	6:1	5.9:1 (**4**)	3.7
[Ru(cod)(cot)] [$Pt(cod)Me_2$] (**D/E**)	1:1	1:1 (**5**)	3.6

C_3H_5)]/[$CpPtMe_3$]@MOF-5 (**2**) were published in an earlier report (the data of **3**–**4** are quite similar).[1b] The observed ^{13}C MAS-NMR signals of **1** can be clearly assigned to the carbon atoms in the two different intercalated molecules (see Table 2) matching the literature data of the precursor molecules in C_6D_6.[15] The MOF-5 carbon signals can be observed at 174.9 (*C*OO), 137.0 [*C*(COO)] and 131 (C_6H_4) ppm. Furthermore, the signal at –18.8 ppm shows the typical splitting due to Pt–C coupling with a coupling constant of 706 MHz.[16] The ^{195}Pt MAS-NMR spectrum of sample **1** exhibits one signal at –5224.9 ppm which is also consistent with the literature data of [$CpPtMe_3$].[16] Small deviations in the ^{13}C MAS-NMR shifts of the Fe precursor in MOF-5, when loaded separately and together with the Pt precursor, possibly arise from the relatively broad signals in solid-state NMR spectroscopy. The ^{13}C MAS-NMR spectrum of sample **5** is given in Figure 2. Besides the unchanged carbon signals of the MOF-5 host material at 175.6, 136.8 and 131.6 ppm (marked by asterisks), the carbon resonances of the included precursors [Ru(cod)(cot)] and [$Pt(cod)Me_2$] can be observed clearly (see Table 2). The chemical shifts of the precursor signals correspond to the ^{13}C MAS-NMR literature data of the precursor molecules in C_6D_6 solution[17,18] confirming that both precursors were adsorbed chemically unchanged. Unfortunately, due to technical difficulties, the ^{195}Pt MAS-NMR resonance signal of the adsorbed Pt precursor of **5** could not be detected. However, in the ^{13}C-MAS-NMR spectrum, a typical Pt–C coupling of the carbon signal corresponding to the methyl groups of [$Pt(cod)Me_2$] was observed with a value of $J_{Pt,C}$ = 785 MHz which also matches the literature data.[18]

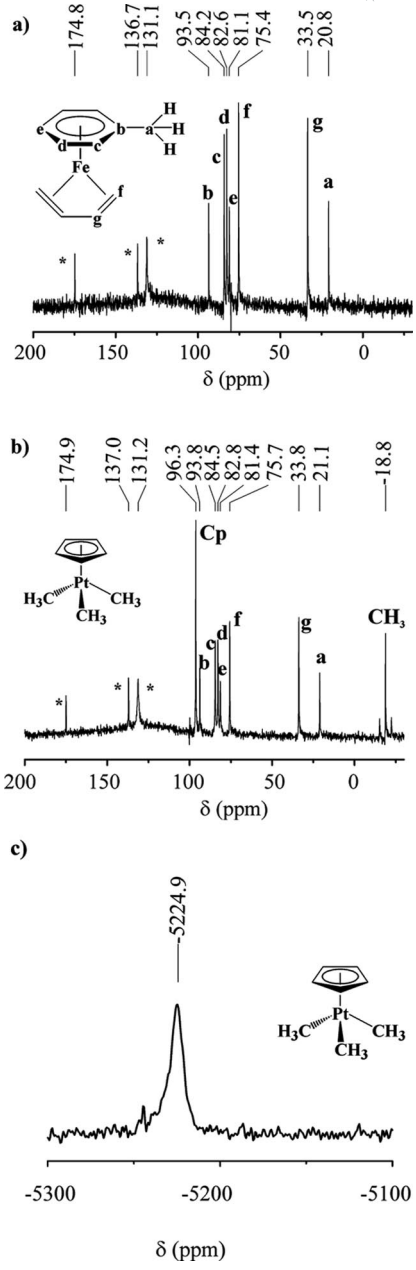

Figure 1. (a) ^{13}C MAS-NMR spectrum of [Fe(η^6-toluene)(η^4-C_4H_6)] (**A**), (b) ^{13}C MAS-NMR spectrum of [Fe(η^6-toluene)(η^4-C_4H_6)]/[$CpPtMe_3$]@MOF-5 (sample **1**). The corresponding ^{195}Pt MAS-NMR spectrum of **1** is given in the Supporting Information (Figure S1). Resonances arising from the MOF matrix are marked by asterisks.

Figure 3 shows the PXRDs of the composites **1** and **2** compared to the PXRD of pure, argon filled MOF-5. The PXRDs of the composites **3** and **4** were akin to the PXRD of **2**. When compared to the diffractogram of empty MOF-5 (Figure 3, c), the PXRDs of the composite materials **1** and **2** (Figure 3, a and b) show *all* typical MOF-5 reflections but with very different intensity ratios than in pure, empty MOF-5. The PXRD of pure MOF-5 (Figure 3, c) shows the reflections of 2θ of 13.7° (400) and 15.4° (420), the latter being the most intense. In the PXRD of **1** and **2**, the most intense reflection is the (511) reflection at 17.8° with the reflections at 15.4°(420) and 19.4° (440) exhibiting also rather high intensities and one new reflection at 11.9° (marked by an asterisk) with about the same intensity. These observed changes in the PXRDs of composites **1** and **2**, when compared with pure MOF-5, must be due to a high degree of disorder in the composite structure. The loading of MOF-5 with two different precursor molecules clearly leads to an adsorbate "structure" without long range translational order. Similar observations have been made upon

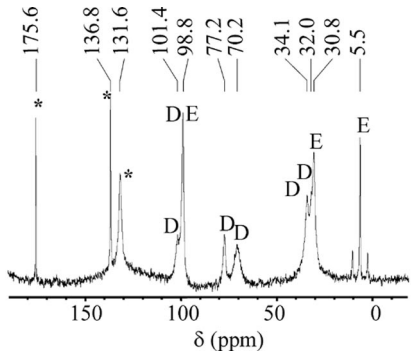

Figure 2. ^{13}C MAS-NMR spectrum of the composite material [Ru(cod)(cot)]/[Pt(cod)Me_2]@MOF-5 (**5**). Resonances arising from the MOF matrix are marked by asterisks.

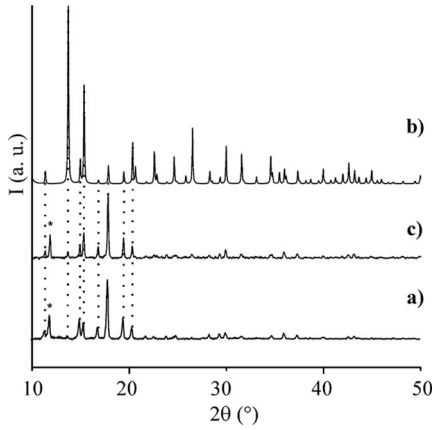

Figure 3. Powder X-ray diffractograms of a) [Fe(η^6-toluene)(η^4-C_4H_6)]/[CpPtMe_3]@MOF-5 (**1**), b) [CpPd(η^3-C_3H_5)]/[CpPtMe_3]-@MOF-5 (**2**) and c) pure MOF-5.

absorption of highly disordered solvent molecules in MOF-5.[19] This also indicates that the distribution of the two different precursors throughout MOF-5 is very likely to be statistical. However, a completely uniform mixture of both components throughout the host framework's cavities, as would be the case in a "real" solvent rather than in a solid solvent cage as the MOF-5 matrix may be viewed, is most likely not obtained. Different adsorption properties of the precursors and preferred intermolecular interactions between precursor molecules of the same kind have to be taken into account. The single new reflection observed in the PXRDs of **1** and **2** compared to the PXRD of MOF-5 could be attributed to the absorption of the organometallic molecules but could not be indexed. Since all the typical (and indexed) MOF-5 reflections are preserved in the PXRDs of **1** and **2**, it can still be concluded that the host structure does not change upon loading with two kinds of precursor molecules and remains mostly intact.

The PXRD of composite **5** compared with that of pure, argon filled MOF-5 is given in Figure 4. In comparison with the PXRD of pure MOF-5, a drastic decrease in the overall reflection intensities can be observed in the PXRD of the composite **5**. The PXRD of [Ru(cod)(cot)]/[Pt(cod)-Me_2]@MOF-5 (**5**) exhibits the prominent MOF-5 reflections at 13.7° and 15.4° in about the same intensity ratio as in the pure activated MOF-5. The intensity of the reflection at 9.7° in the PXRD of [Ru(cod)(cot)]/[Pt(cod)Me_2]@-MOF-5 is reduced when compared with the intensities of the reflections at 13.7° and 15.4°. The decrease of the intensities of MOF-5 reflections below $2\theta = 10°$ is a result of the loading of the MOF-5 cavities.[20] Remarkably, the characteristic MOF-5 reflection at 6.9° is not observed for **5**. However, the single new reflection at 11.9° that was also observed in the PXRDs of **1** and **2**, is also present in the PXRD of **5**. The drastic decrease of the MOF-5 reflections in the PXRD of [Ru(cod)(cot)]/[Pt(cod)Me_2]@MOF-5 when compared with the PXRD of the parent MOF-5 material, together with a much lower signal-to-noise ratio is a consequence of the loading with the precursor compounds containing heavy atoms (strong X-ray scattering). This disorder expectedly changes the PXRD of the composite more dramatically when the loading is performed below the saturation level of forming a well ordered adsorbate structure as in the case of single loadings, i.e. ferrocene inside MOF-5.[14] To verify the unchanged nature of the host material upon inclusion of the Ru and Pt precursor molecules, the precursors were removed from the composite [Ru(cod)-(cot)]/[Pt(cod)Me_2]@MOF-5 by immersion in dry *n*-pentane (both precursor components dissolve well in *n*-pentane) and filtering the solution. The procedure was repeated three times until the supernatant remained colourless. An off-white powder was obtained which, after careful drying in vacuo (10^{-3} mbar) at 100 °C overnight, exhibited the PXRD presented in part b of Figure 4. The PXRD of the powder is identical to the PXRD of pure, empty MOF-5 (Figure 4, a). N_2 sorption measurements gave the typical Langmuir surface area of MOF-5 with a value of 3300 $m^2 g^{-1}$ and the removal of the precursor molecules

Table 2. Assignment of the MAS-NMR spectroscopic data of [Fe(η^6-toluene)(η^4-C_4H_6)]/[CpPtMe_3]@MOF-5 (**1**) and [Ru(cod)(cot)]/[Pt(cod)Me_2]@MOF-5 (**5**).

Precursor adsorbed inside MOF-5 of composites **1**, **5**	^{13}C δ / ppm	^{195}Pt δ / ppm
[Fe(η^6-toluene)(η^4-C_4H_6)] (1)	93.8 (η^6-$C_6H_5CH_3$), 84.5 (η^6-$C_6H_5CH_3$), 82.8 (η^6-$C_6H_5CH_3$), 81.4 (η^6-$C_6H_5CH_3$), 75.7 (η^4-C_4H_6), 33.8 (η^4-C_4H_6), 21.1 (η^6-$C_6H_5CH_3$)	–
[CpPtMe_3] (1)	96.3 (η^5-C_5H_5), –18.8 [CH_3, J(Pt,C) = 706 MHz]	–5224.9
[Ru(cod)(cot)] (5)	101.4 (cot, olef.), 98.8 (cot, olef.), 77.2 (cot, olef.), 70.2 (cod, olef.), 34.1 (cod, aliph.), 32.0 (cot, aliph.)	–
[Pt(cod)Me_2] (5)	98.8 (cod, olefin), 30.8 (cod, aliph.), 5.5 [CH_3, J(Pt–C) = 785 MHz]	–

was verified by an FTIR spectroscopic measurement. This proves that the MOF-5 host framework of the composite [Ru(cod)(cot)]/[Pt(cod)Me_2]@MOF-5 remains unchanged upon inclusion of the Pt and Ru precursor molecules, although the PXRD of [Ru(cod)(cot)]/[Pt(cod)Me_2]@MOF-5 (**5**) looks rather different from that of pure MOF-5.

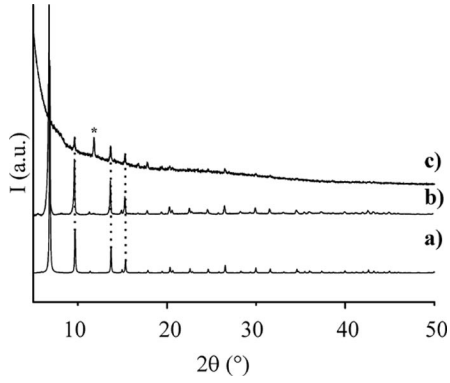

Figure 4. Powder X-ray diffractograms of a) pure MOF-5, b) MOF-5 obtained after quantitative removal of the precursors from composite **5** and c) composite material [Ru(cod)(cot)]/[Pt(cod)-Me_2]@MOF-5 (**5**).

2. Hydrogenation of the Composite Material [Ru(cod)(cot)]/[Pt(cod)Me_2]@MOF-5 under Mild Conditions

Composite **5** was chosen as a representative example for the investigation of co-hydrogenolysis of two different metal precursors intercalated in MOF-5 because we have already studied the hydrogenolysis of [Ru(cod)(cot)]@MOF-5 in some detail.[1d] Moreover, composite **5** exhibited quite a defined precursor ratio of [Pt(cod)Me_2]/[Ru(cod)(cot)] = 1:1, possibly allowing the formation of crystalline $Pt_{50}Ru_{50}$ alloy nanoparticles when exposed to hydrogen. Since PtRu alloys are very active hydrogenation catalysts, rather gentle conditions were chosen for the first attempt of co-hydrogenolysis of [Ru(cod)(cot)] and [Pt(cod)Me_2] in MOF-5, in order to avoid decomposition of the host framework MOF-5. The composite was exposed to a stream of hydrogen (1 bar, 1 sccm) at 25 °C for 10 min until a colour change of the material from yellow to dark-brown was observed. The resultant material is denoted as **6**. The ^{13}C MAS-NMR spectrum of **6** is given in Figure 5. The spectrum exhibits the carbon signals of unchanged MOF-5 at 175.2, 136.7 and 131.0 ppm. In addition, the ^{13}C MAS-NMR signals of the [(η^6-arene)Ru(cod)] complex with the MOF-5 bdc linkers at 178.5, 91.0, 83.2, 68.3 and 33.4 ppm could also be detected. Note that formation of this complex was also observed when [Ru(cod)(cot)]@MOF-5 was exposed to H_2 under mild conditions.[1d] The signal at δ = 27.3 ppm was assigned to incompletely desorbed cyclooctane, stemming from the side product of hydrogenolysis of [Ru(cod)(cot)]. Furthermore, the ^{13}C MAS-NMR spectrum of **6** shows the carbon signals of the Pt precursor [Pt(cod)Me_2] (**E**) unchanged. The powder X-ray diffractogram of the composite (see Supporting Information, Figure S2) looks somewhat different from the PXRD of **5** before hydrogen treatment. However, it exhibits the typical MOF-5 PXRD reflections in the same intensity ratios as in the parent MOF-5 material hinting at an unchanged MOF-5 matrix. Additional Bragg reflections from Ru, Pt or RuPt were not observed however. Therefore, no conclusions about the formation of nanoparticles inside the MOF-5 cavities can be made from the PXRD of **6**. A determination of the Langmuir surface area could not be carried out because of the remaining Pt precursor molecules (**E**) in the composite (desorption during the experiment). From the agreement of the peak position of pure MOF-5 with the co-hydrogenolysis product **6** it can be concluded that the MOF-5 matrix remained mostly unchanged upon *gentle* hydrogen treatment.

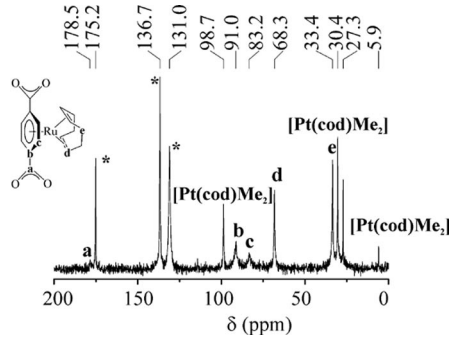

Figure 5. ^{13}C-MAS-NMR of composite **6** obtained by gentle hydrogenation of [Ru(cod)(cot)]/[Pt(cod)Me_2]@MOF-5 (**5**).

3. Hydrogenation of [Ru(cod)(cot)]/[Pt(cod)Me_2]@MOF-5 under Harsh Conditions

In order to achieve quantitative co-hydrogenolysis of both precursors [Ru(cod)(cot)] (**D**) and [Pt(cod)Me_2] (**E**) in MOF-5, the hydrogen treatment was performed at elevated temperature and pressure. Keeping in mind the catalytic activity of PtRu alloys in hydrogenation reactions, the treatment was, however, performed under somewhat milder conditions than in the case of hydrogenolysis of [Ru(cod)-(cot)]$_{3.5}$@MOF-5 to give Ru@MOF-5.[1d] Composite **5** was treated with 1 bar H_2 at 150 °C for 3 h only, rather than 3 d at 3 bar. Thereupon a colour change of from yellow to black was observed. Volatile by-products were desorbed in vacuo. The obtained product is denoted as composite **7**. From N_2 sorption measurements the Langmuir surface area of **7** was recorded as 380 $m^2 g^{-1}$ which is a very poor value compared with the surface area of the starting material MOF-5 of 3300 $m^2 g^{-1}$. From elemental analyses/AAS results, the molar ratio in the composite was determined as Ru/Pt = 1:1 ($\pm$ 0.1). Figure 6 presents the ^{13}C MAS-NMR spectrum of **7**. The signals of unchanged MOF-5 linkers are observed at 175.0, 136.9 and 130.7 ppm. In addition, five new rather broad signals at 186.3, 45.1, 41.1 and 29.6 ppm can be observed that can neither be assigned to remaining Ru or Pt precursor molecules nor to the discussed complex of the type [(η^6-arene)Ru(cod)] with MOF-5 bdc linkers. The ^{13}C carbon signals of these compounds are completely

missing, indicating quantitative hydrogenolysis of [Ru(cod)(cot)] and [Pt(cod)Me_2] in MOF-5. The comparison with the ^{13}C MAS-NMR spectrum of *cis*/*trans*-1,4-cyclohexanedicarboxylic acid, which is a possible hydrogenation product of the MOF-5 bdc linkers (Figure 6, b), shows that the signals in the ^{13}C MAS-NMR spectrum of **7** are likely to originate from hydrogenated MOF-5 bdc linkers. The signal at δ = 27.2 ppm most probably stems from incompletely desorbed cyclooctane which is a side product in hydrogenolysis of the Pt and Ru precursor molecules. Obviously complete conversion of the embedded Ru and Pt precursor molecules was achieved but associated with part hydrogenation of the MOF-5 linkers, however. Compared with the carbon signals in the ^{13}C MAS-NMR spectrum of the free acid molecules (Figure 6, b), the corresponding signals of **7** are rather broad. This indicates that the hydrogenated linkers remain bound to the Zn_4O units of the MOF-5 and are therefore more rigid in the solid matrix than in the case of free acid molecules (solid state). Recently, the synthesis of a metal-organic framework based on Zn_4O tetrahedrons linked by cyclohexanedicarboxylate was reported.[21] From these comparisons we conclude that the chemical bonding situation in the MOF-type matrix of **7** might be more or less intact and similar to MOF-5 even though a significant fraction of the bdc linkers were converted to cyclohexanedicarboxylate.

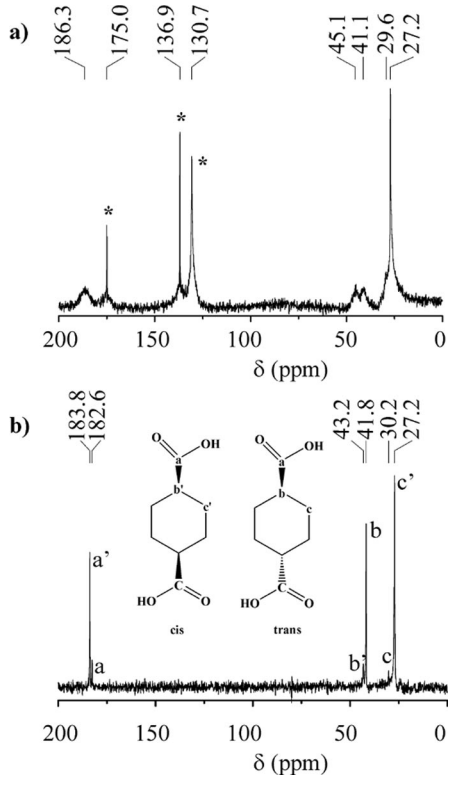

Figure 6. ^{13}C MAS-NMR spectra of a) composite **7** and b) a reference spectrum of *cis*-/*trans*-1,4-cyclohexandedicarboxylic acid.

The hydrogenation of the linkers possibly occurred in the close environment of the PtRu species. Note that we already reported on H/D exchange at the bdc linkers in case of Ru@MOF-5.[1d] However, upon hydrogenolysis of [Ru(cod)(cot)]$_{3.5}$@MOF-5 (150 °C, 3 bar H_2, 3 d) no hydrogenation of the MOF-5 linkers was indicated by the corresponding ^{13}C MAS-NMR spectrum.[1d] Also, the hydrogenation of the composites [Pt(cod)Me_2]@MOF-5 or [CpPtMe_3]@MOF-5[1d] to form the material Pt@MOF-5 did not show any hydrogenated bdc linkers (see Supporting Information, Figure S3). The formation of Pt nanoparticles in the related matrix [$Zn_4O(btb)_3$] (MOF-177; btb = 1,3,5-benzenetribenzoate) by the hydrogenolysis of {Pt[η^5-$C_5H_4(CH_3)$]-$(CH_3)_3$} was shown previously.[1e] The authors did not detect hydrogenated btb in the corresponding ^{13}C MAS-NMR spectroscopy. Obviously, the Ru/Pt case here is different and the simultaneous presence of both Ru and Pt leads to partial hydrogenation of the MOF-5 linkers. The superior catalytic activity of alloyed RuPt catalysts in hydrogenation of benzene, in contrast to a pure Ru or Pt catalyst has been reported in the literature.[22] We suggest, that this effect might be also the reason for the substantial hydrogenation of the MOF-5 linkers in the case discussed here.

The PXRD of composite material **7** (top) in comparison with the PXRD of pure MOF-5 (bottom) is given in Figure 7. The PXRD of **7** shows only very weak remaining reflections of the host matrix MOF-5, indicating a great loss of crystallinity of the host matrix most probably due to hydrogenation of a fraction of the MOF-5 bdc linkers as discussed above. In addition, four new very broad Bragg reflections can be observed with the most prominent centered at 39.84° in 2θ showing a full width at half maximum of 2.5°. These Bragg reflections have been assigned to the metal nanospecies formed upon quantitative hydrogenolysis of [Ru(cod)(cot)] and [Pt(cod)Me_2] in MOF-5. Comparison of these reflections with the simulated PXRD patterns of bulk hexagonal (hcp) Ru and face centred cubic (fcc) Pt metal (Figure 7) shows that the reflections cannot be assigned to hcp Ru nanoparticles. The reflections rather point to a fcc structure close to bulk phase platinum. However, the observed value of 39.84° in 2θ is slightly shifted from the reference Pt(111) reflection expected at 39.76° in 2θ. This situation has been observed before for PtRu nanoalloys.[23a] In alloyed PtRu nanoparticles, the smaller Ru atoms substitute the larger Pt atoms in the Pt fcc lattice which causes a slight shrinking of the lattice parameters and therefore results in a shifting of the corresponding Bragg reflections to larger 2θ values. The shift is dependent on the atomic ratios of Pt and Ru in the alloy and becomes more pronounced with increasing Ru content. Up to a limit of 62 atom-% of Ru, the (fcc) structure of Pt is maintained and a solid solution (homophase) is formed (Supporting Information, Figure S4) then, at up to 80 at.% of Ru, a biphasic mixture of (hcp) Ru and (fcc) Pt exists and above 80 at.% of Ru, the (hcp) Ru structure is adopted.[23b] In particular, alloyed $Pt_{50}Ru_{50}$ nanoparticles with a size of 3.5 nm exhibited a (111) reflection at 39.80°.[23a] Therefore we assigned the observed Bragg reflection at 39.84° to alloyed $Pt_{50}Ru_{50}$ nanoparticles which is also in agreement with the elemental analysis of the composite exhibiting an equimolar ratio of Pt to Ru. From the FWHM of this re-

flection a crystallite size of 3.8 nm was calculated with the standard Scherrer equation. This size, which is much larger than observed for Ru@MOF-5 before,[1d] of course exceeds the diameter of the (larger) MOF-5 cavity of 1.5 nm. The host framework is distorted by partial hydrogenation of the MOF-5 bdc linkers which certainly favours particle growth. A TEM image of the composite **7** is given in Figure 8. The metal nanoparticles can be observed as darker spots distributed over the host matrix due to the higher contrast in the electron beam and were found to be in a size range of 4–6 nm. The corresponding SAED pattern exhibits broad and diffuse diffraction rings. This limits the accuracy in the calculation of the lattice constants *d* of the metal particle. As discussed above, the shrinkage of the lattice size due to possible alloyed Pt/Ru particles causes only slight deviations in the PXRD peak positions in comparison with pure Pt which is also the case for the electron diffraction data. The EDX analysis, by focusing on the displayed area, clearly reveals, however, the presence of both Ru and Pt. Nevertheless, an accurate determination of the Ru:Pt ratio was not possible on this scale of imaging. In order to check the distribution of Ru and Pt throughout the composite material, several TEM images and EDX spectra of different sample regions were taken. The data (see Supporting Information, Figures S4 and S5) suggest some variation of the Ru/Pt ratio in different areas of the matrix but confirm the alloying deduced from PXRD. Because of the disintegrated, amorphous MOF matrix, we did not study in detail the 3D-distribution of the metal particles over the imaged specimen in order to rigorously address the question of segregation of the particles to the other surface of the matrix.[24]

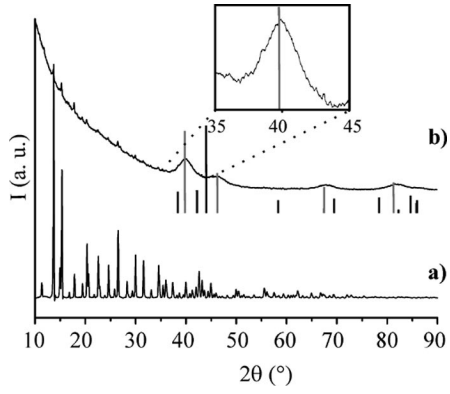

Figure 7. Powder-X-ray diffractograms of a) pure MOF-5 and b) Ru/Pt@MOF-5, denoted as composite **7**. Vertical lines: selected peak positions for Ru (black; JPDS reference No. 6-00663) and Pt (gray; JPDS reference No. 4-0802).

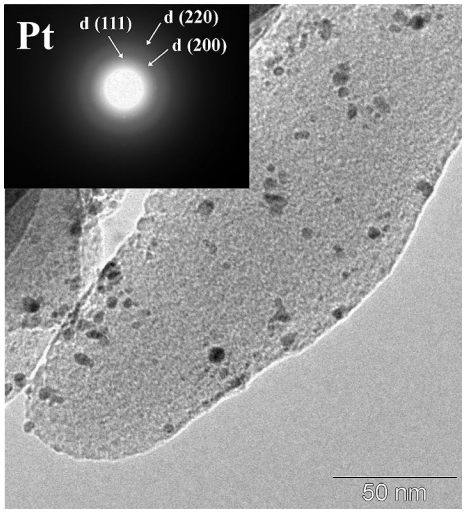

Figure 8. TEM image of a representative area of composite **7** with the SAED pattern as an insert at the upper left (for EDX spectrum see Supporting Information, Figure S5). Only the Pt homophase was detected with some indication of a solid solution of Ru (slight shrinking of the fcc Pt lattice spacings).

Conclusions

The simultaneous loading of MOF-5 with two metal precursor was investigated using the following combinations [Fe(η^6-toluene)(η^4-C_4H_6)]/[$CpPtMe_3$], [$CpPd(\eta^3$-C_3H_5)]/[$CpPtMe_3$] and [Ru(cod)(cot)]/[$Pt(cod)Me_2$]. The adjustment of a defined molar ratio between the adsorbed precursor molecules in MOF-5, which is an important prerequisite for the synthesis of functional alloys, proved to be difficult for loading under mild conditions (room temperature, reduced pressure). However, quantitative adsorption below the saturation limit using an equimolar ratio of the precursors [Ru(cod)(cot)] and [$Pt(cod)Me_2$] led to the desired equimolar loading with a total of about 3.6 mol of precursor per MOF-5formula unit which is quite similar to that observed for a single precursor loading in case of [Ru(cod)(cot)]$_{3.5}$@MOF-5.[1d] In a similar way, it should be possible to load MOF-5 and other suitable MOFs or porous coordination polymers, in general, with two different precursor components in various molar ratios in a controlled way. The conversion of the adsorbed precursors to yield alloyed Ru/Pt nanoparticles supported by the MOF-5 matrix was investigated using the composite [Ru(cod)(cot)]/[$Pt(cod)Me_2$]-@MOF-5 (**5**) as a representative example. Quantitative decomposition of the precursors was achieved, however, by partial hydrogenation of the MOF-5 bdc linkers at the same time but this is not observed for the single metal loaded M@MOF-n (M = Ru, Pd, Pt; *n* = 5, 177).[1a,1d,1e] Analysis of the resultant composite material by TEM revealed a nonuniform distribution of Ru and Pt throughout the MOF-5 host. Although elemental and AAS analysis of the composite gave an over-all Pt/Ru = 1:1 ratio, EDX analysis points to enrichment of Ru in some parts of the nanocrystallites of the composite material. This hints at an also nonuniform distribution of the Ru and Pt precursor molecules in MOF-5, prior to the hydrogenolysis. In addition, the hydrogenolysis of the Ru precursor obviously occurs faster than that of the Pt precursor, leading to the preformation of Ru particles which could act as catalysts for the decomposition of the Pt precursor. Thus, hydrogenation of [Ru(cod)(cot)]/[$Pt(cod)Me_2$]@MOF-5 under mild conditions led to partial decomposition of the Ru precursor molecules, whereas the Pt precursor molecules remained unchanged. The forma-

tion of Ru nanoparticles prior to the start of formation of Pt clusters might lead to Ru enriched parts of the host framework and this, furthermore, also complicates the formation of a nanoalloy. The PXRD (and SAED) of the obtained Pt/Ru@MOF-5 composite exhibits reflections assignable to a (fcc) Pt homophase with the reflection maxima slightly shifted to higher 2θ values, however. This finding is a hint at possibly alloyed Pt/Ru species, since PtRu alloys adopt the (fcc) Pt structure up to 62 at.% of Ru. Such PtRu alloying to some extent is also supported by the observation of the hydrogenated bdc linkers. However, further TEM and also XAS measurements need to be performed to examine the nature of the resultant species in more detail and the latter is currently under investigation.

Experimental Section

Analytical and Spectroscopic Methods: Elemental analysis was performed by the Analytical Laboratory of the Catalysis Research Centre of Süd Chemie AG, Heufeld, Germany. The measurements were performed by standard protocols employing Inductively Coupled Plasma Atom Emission Spectroscopy (ICP-AES). N_2 sorption measurements were performed using a Quantachrome Autosorp-1 MP instrument and optimised protocols. FTIR spectra were recorded as KBr pellets using a Perkin–Elmer 1720x spectrometer. The samples were prepared in a glove box (MBraun; O_2 and H_2O continuously monitored with levels below 1 ppm). KBr was dried at 300 °C at 10^{-3} mbar for 16 h prior to specimen preparation. All X-ray powder diffractograms were recorded on a D8-Advance-Bruker-AXS-diffractometer (Cu-K_α radiation, 1.54178 Å) in θ–2θ geometry and with a position sensitive detector. All powder samples were filled into glass capillaries (ø = 0.7 mm) in the glove box and sealed prior to the measurements. TEM measurements were carried out on a Hitachi-H-8100 instrument (accelerating voltage up to 200 kV) using carbon coated Cu grids. Solid state MAS-NMR spectra were recorded on a Bruker DSX 400 MHz instrument in ZrO_2-rotors (Ø = 2.5 mm) with rotational frequencies of 20 kHz. All ^{13}C MAS-NMR spectra were measured by applying a cross polarisation (CP) pulse programs based on standard parameters written by H.-J. Hauswald at the Analytical Chemistry Department at the Ruhr-University Bochum.

Starting Material Synthesis: The following precursors were synthesised according to the literature: $[CpPtMe_3]$,[25] $[CpPd(\eta^3\text{-}C_3H_5)]$,[26] [Ru(cod)(cot)][27] and $[Pt(cod)Me_2]$.[28]

$[Fe(\eta^6\text{-toluene})(\eta^4\text{-}C_4H_6)]$ was kindly provided by the group of Prof. U. Zenneck, University of Erlangen-Nürnberg. MOF-5 was also synthesised according to a known literature procedure published by Yaghi et al.[29] Colourless MOF-5 crystals typically 2 mm in size were activated by stirring in chloroform for 12 h and careful drying and degassing at 110 °C in dynamic vacuo (10^{-3} mbar) for 16 h. Before all further manipulations, the powder was stored under an inert gas atmosphere in a glove box. The MOF-5 material was characterised by XRD and standard N_2-sorption measurements at 77 K. The results were in good agreement with the known literature data.

Preparation of $[Fe(\eta^6\text{-toluene})(\eta^4\text{-}C_4H_6)]/[CpPtMe_3]$@MOF-5(1): Dry MOF-5 powder (100 mg, 0.13 mmol), $[CpPtMe_3]$ (120 mg, 0.39 mmol) and $[Fe(\eta^6\text{-toluene})(\eta^4\text{-}C_4H_6)]$ (79 mg, 0.39 mmol) were placed in three different glass vials in a Schlenk tube. The tube was evacuated for 5 min (10^{-3} mbar), sealed and kept at 25 °C for 12 h. A red-brown composite denoted as $[Fe(\eta^6\text{-toluene})(\eta^4\text{-}C_4H_6)]/[CpPtMe_3]$@MOF-5 was obtained; yield 212 mg (95% based on the amounts of absorbed Fe and Pt precursor molecules). Elemental analysis (wt.-%): Fe 7.5, Pt 18.5, Zn 16.9, C 43.1, H 3.9 (O 10.1 calcd. from difference to 100%); deduced number of precursor molecules per MOF-5 cavity: n($[Fe(\eta^6\text{-toluene})(\eta^4\text{-}C_4H_6)]$): n($[CpPtMe_3]$) = 2.2:1.6 (±0.1), resulting overall ratio of 1.4:1 (±0.1). IR (KBr): $\tilde{\nu}_{max}$ = 3026 (w), 2970 (w), 2920 (w), 1605 (s), 1505 (m), 1395 (vs), 1157 (vw), 1018 (w), 1105 (vw), 909 (vw), 885 (vw), 824 (w), 746 (m), 731 (m), 695 (w), 576 (w), 517 (m), 465 (vw) cm^{-1}. ^{13}C MAS NMR: δ = 174.9 [(*C*OO) MOF-5], 137.0 [*C*(COO) MOF-5], 131.2 (C_6H_4 MOF-5), 96.3 {$[Pt(\eta^5\text{-}C_5H_5)(CH_3)_3]$}, 93.8 {$[Fe(\eta^6\text{-}C_6H_5CH_3)(\eta^4\text{-}C_4H_6)]$}, 84.5 {$[Fe(\eta^6\text{-}C_6H_5CH_3)(\eta^4\text{-}C_4H_6)]$}, 82.8 {$[Fe(\eta^6\text{-}C_6H_5CH_3)(\eta^4\text{-}C_4H_6)]$}, 81.4 {$[Fe(\eta^6\text{-}C_6H_5CH_3)(\eta^4\text{-}C_4H_6)]$}, 75.7 {$[Fe(\eta^6\text{-}C_6H_5CH_3)(\eta^4\text{-}C_4H_6)]$}, 33.8 {$[Fe(\eta^6\text{-}C_6H_5CH_3)(\eta^4\text{-}C_4H_6)]$}, 21.1 {$[Fe(\eta^6\text{-}C_6H_5CH_3)(\eta^4\text{-}C_4H_6)]$}, –18.8 {$J_{Pt,C}$) = 706 MHz, $[Pt(\eta^5\text{-}C_5H_5)(CH_3)_3]$} ppm. ^{195}Pt MAS NMR: δ = –5224.9 {$[Pt(\eta^5\text{-}C_5H_5)(CH_3)_3]$} ppm. PXRD: capillary: 2 θ [°] (intensity): 11.3 (11,8), 11.8 (37.2), 13.7 (10.2), 14.9 (20.8), 15.3 (40.2), 16.8 (18.1), 17.8 (100), 19.4 (32.2), 20.3 (19.0), 22.5 (5.3), 23.8 (5.6), 24.8 (5.1), 26.4 (6.3), 29.3 (7.0), 30.0 (13.5), 31.5 (6.1), 34.5 (4.8), 36.0 (9.7), 37.3 (6.7), 40.0 (3.2), 42.5 (5.6), 43.1 (6.6).

Preparation of $[CpPd(\eta^3\text{-}C_3H_5)]/[CpPtMe_3]$@MOF-5 (2–4): In a series of three loading experiments, samples of dry MOF-5 powder (50 mg, 0.065 mmol), $[CpPd(\eta^3\text{-}C_3H_5)]$ (*x* mg) and $[CpPtMe_3]$ (*y* mg) (Table 3) were placed in two different glass vials in a Schlenk tube. The tube was evacuated for 5 min (10^{-3} mbar) then sealed and kept in the dark at 25 °C for 4 h. Dark red composites, denoted as $[CpPd(\eta^3\text{-}C_3H_5)]/[CpPtMe_3]$@MOF-5 exhibiting different precursor ratios were obtained. Elemental analysis: see Table 3. IR (KBr): $\tilde{\nu}_{max}$ = 2961 (w), 2898 (w), 2814 (vw), 1603 (s), 1504 (m), 1395 (vs), 1258 (w), 1215 (w), 1156 (vw), 1103 (w), 1015 (m), 910 (vw), 882 (vw), 823 (w), 793 (m), 766 (m), 744 (s), 574 (m), 550 (w), 514 (m) cm^{-1}. ^1H MAS NMR: δ = 8.5 (C_6H_4, MOF-5), 5.6 {$[Pd(\eta^5\text{-}C_5H_5)(\eta^3\text{-}C_3H_5)]$, $[Pt(\eta^5\text{-}C_5H_5)(CH_3)_3]$}, 4.7 {$[Pd(\eta^5\text{-}C_5H_5)(\eta^3\text{-}C_3H_5)]$}, 3.4 {$[Pd(\eta^5\text{-}C_5H_5)(\eta^3\text{-}C_3H_5)]$}, 2.1 $[Pd(\eta^5\text{-}C_5H_5)(\eta^3\text{-}C_3H_5)]$, 1.1 ($[Pt(\eta^5\text{-}C_5H_5)(CH_3)_3]$) ppm. ^{13}C MAS-NMR: δ = 175.0 (*C*OO MOF-5), 137.0 [*C*(COO) MOF-5], 131.1 (C_6H_4 MOF-5), 99.5 {$[Pt(\eta^5\text{-}C_5H_5)(CH_3)_3]$}, 94.7 {$[Pd(\eta^5\text{-}C_5H_5)(\eta^3\text{-}C_3H_5)]$}, 46.3 {$[Pd(\eta^5\text{-}C_5H_5)(\eta^3\text{-}C_3H_5)]$}, –19.1 {$[Pt(\eta^5\text{-}C_5H_5)(CH_3)_3]$} ppm. ^{195}Pt MAS NMR: δ = –5216.9 {$[Pt(\eta^5\text{-}C_5H_5)(CH_3)_3]$} ppm. PXRD: capillary: 2 θ [°] (intensity): 11.3 (12.5), 11.9 (40.1), 13.7 (5.6), 14.9 (32.8), 15.3 (27.8), 16.8 (20.3), 17.8 (100), 19.4 (35.1), 20.3 (19.8), 21.7 (5.0), 22.6 (4.0), 23.9 (4.9), 24.9 (5.9), 28.3 (7.6), 29.3 (8.8), 30.0 (10.4), 31.6 (4.7), 34.7 (5.8), 36.0 (9.6), 37.3 (6.4), 40.0 (2.8), 42.6 (3.7), 43.2 (4.6).

Table 3. Amounts of *x* mg $[CpPd(\eta^3\text{-}C_3H_5)]$ and *y* mg $[CpPtMe_3]$ applied in the loading experiments of MOF-5 to yield composites **2**–**4** and the corresponding elemental analysis data.

	Sample **2**	Sample **3**	Sample **4**
$CpPd(\eta^3\text{-}C_3H_5)$ (**C**)	100 mg (0.47 mmol)	100 mg (0.47 mmol)	223 mg (1.04 mmol)
$[CpPtMe_3]$ (**B**)	144 mg (0.47 mmol)	50 mg (0.16 mmol)	53 mg (0.17 mmol)
Composite M wt.-%	Pd 16.4 Pt 11.1 Zn 16.8	Pd 18.7 Pt 8.3 Zn 16.7	Pd 20.8 Pt 6.5 Zn 16.5
C,H wt.-%	C 38.9, H 3.2	C 39.5, 3.2	C 40.0, H 3.2
O wt.-%[a]	O 13.6	O 13.6	O 13.0

[a] Calculated from difference to 100%.

Preparation of [Ru(cod)(cot)]/[Pt(cod)Me$_2$]@MOF-5 (5): In a typical experiment, a sample of dry MOF-5 powder (50 mg, 0.065 mmol), [Pt(cod)Me$_2$] (53 mg, 0.16 mmol) and [Ru(cod)(cot)] (50 mg, 0.16 mmol) were placed in a Schlenk tube in two different glass vials. The tube was evacuated for 10 min, sealed (10^{-5} mbar) and then kept at 25 °C until complete absorption of both precursors was observed (duration: 48 h). A yellow powder, denoted as [Ru(cod)(cot)]/[Pt(cod)Me$_2$]@MOF-5 was obtained; yield 151 mg (99% based on both precursor compounds). Elemental analysis (wt.-%): Ru 9.8, Pt 17.0, Zn 13.5, C 41.3, H 4.39 (O 14.0 calcd. From difference to 100%); deduced number of precursor molecules per MOF-5 cavity: n{[Ru(cod)(cot)]}:n{[Pt(cod)Me$_2$]} = 1.9:1.7(± 0.1), resultant overall stoichiometric ratio of [Ru(cod)(cot)]:[Pt(cod)Me$_2$]: 1:1 (± 0.1). IR (KBr): $\tilde{\nu}_{max}$ = 3057 (vw), 2994 (vw), 2920 (w), 2869 (w), 2833 (vw), 2792 (vw), 1953 (w), 1603 (s), 1504 (m), 1393 (vs), 1265 (w), 1156 (w), 1092 (w), 1017 (w), 977 (w), 883 (vw), 858 (vw), 821 (w), 745 (m), 574 (w), 514 (w) cm^{-1}. ^{13}C MAS-NMR: δ = 175.6 (*C*OO MOF-5), 136.8 [*C*(COO) MOF-5], 131.6 (C_6H_4 MOF-5), 101.4 {[Ru(cod)(cot)], cot, olef.}, 98.8 {[Ru(cod)(cot)], cot, olef. & [Pt(cod)(CH$_3$)$_2$], cot olef.}, 77.2 {[Ru(cod)(cot)], cot, olef.}, 70.2 {[Ru(cod)(cot)], cod, olefin}, 34.1 {[Ru(cod)(cot)], cod, aliph.}, 32.0 {[Ru(cod)(cot)], cot, aliph.}, 30.8 {[Pt(cod)(CH$_3$)$_2$], cod, aliph.}, 5.5 {[Pt(cod)(*C*H$_3$)$_2$], *J*(Pt–C) = 785 MHz} ppm. PXRD: capillary: 2 θ [°] (intensity): 9.6 (100), 11.8 (99.5), 13.7 (83.5), 15.3 (68.7), 16.7 (48.2), 17.8 (52.4), 19.3 (43.3), 20.3 (44.5), 26.5 (40.0).

Hydrogenation of [Ru(cod)(cot)]/[Pt(cod)(CH$_3$)$_2$]/MOF-5 under Mild Conditions. Preparation of Composite 6: [Ru(cod)(cot)]/[Pt(cod)Me$_2$]@MOF-5 (**5**) (36 mg, prepared as described above) was placed in a glass tube, the glass tube was evacuated (dynamic vacuum, 10^{-2} mbar, 5 min) and the sample then exposed to a stream of hydrogen (1 bar, 1 sccm, 99.999%) at 25 °C for 10 min. A fast colour change from yellow to black was observed; yield 28 mg. Elemental analysis (wt.-%): Ru 9.6, Pt, 16.8, Zn 14.2, C 40.8, H 4.28 (O 14.3 calcd. from difference to 100%) IR (KBr): $\tilde{\nu}_{max}$ = 2918 (s), 2829 (m), 1599 (s), 1506 (m), 1387 (vs), 1261 (m), 1152 (w), 1102 (w), 1083 (w), 1018 (m), 872 (w), 822 (w), 744 (m), 572 (w), 513 (m) cm^{-1}. ^{13}C MAS-NMR: δ = 178.5 {[(η^6-terephthalate)Ru(-cod)], *C*OO} 175.2 (*C*OO MOF-5), 136.7 [*C*(COO) MOF-5], 131.0 (C_6H_4 MOF-5), 98.7 {[Pt(cod)(CH$_3$)$_2$], cot olef.}, 91.0 {[(η^6-terephthalate)Ru(cod)], *C*(COO)}, 83.2 {[(η^6-terephthalate)Ru-(cod)], C_6H_4}, 68.3 {[(η^6-terephthalate)Ru(cod)], cod, olef.}, 33.4 {[(η^6-terephthalate)Ru(cod)], cod, aliph.}, 30.4 {[Pt(cod)(CH$_3$)$_2$], cod, aliph.}, 27.3 (cyclooctane), 5.9 {[Pt(cod)(CH$_3$)$_2$]} ppm. PXRD: capillary: 2θ [°] (intensity): 11.8 (29.6), 13.7 (74.1), 15.3 (100), 16.8 (10.8), 17.8 (35.4), 19.4 (14.2), 20.3 (25.7), 22.6 (17.7), 24.6 (8.5), 25.8 (3.5), 26.5 (18.1), 28.3 (6.6), 30.0 (13.8), 31.6 (12.1), 33.2 (4.3), 34.6 (8.1), 35.5 (4.4), 36.0 (4.4), 37.4 (3.8), 40.0 (3.1), 42.6 (6.4), 43.2 (4.5).

Hydrogenation of [Ru(cod)(cot)]/[Pt(cod)(CH$_3$)$_2$]/MOF-5 under Harsh Conditions. Preparation of Ru/Pt@MOF-5 (7): A sample of [Ru(cod)(cot)]/[Pt(cod)Me$_2$]@MOF-5 (60 mg) was placed in a Fischer-Porter bottle and evacuated for 5 min (dynamic vacuum, 10^{-2} mbar). The bottle was then filled with 1 bar of H_2 gas (99.999%) at 25 °C and heated to 150 °C for 3 h. After cooling to room temperature, H_2 was removed in dynamic vacuum (10^{-2} mbar, 15 min) and the bottle was refilled with Ar; yield 48 mg. Elemental analysis: (wt.-%): Ru 12.6, Pt 21.8, Zn 17.3, C 31.6, H 2.9 (O 16.7 calcd. from difference to 100%); resulting overall molar ratio of Ru/Pt = 1:1 (± 0.1). IR (KBr): $\tilde{\nu}_{max}$ = 2921 (s), 2852 (m), 1581 (s), 1508 (m), 1390 (vs), 1262 (m), 1096 (m), 1020 (m), 878 (vw), 807 (m), 746 (m), 573 (vw), 516 (w) cm^{-1}. ^{13}C MAS NMR: δ = 186.3 (*C*OO, *cis*-/*trans*-1,4-cyclohexanedicarboxylate), 175.0 (*C*OO MOF-5), 136.9 [*C*(COO MOF-5)], 130.7 (C_6H_4 MOF-5), 45.1 [*C*(COO) *cis*-1,4-cyclohexanedicarboxylate], 41.1 [*C*(COO) *trans*-1,4-cyclohexanedicarboxylate], 29.6 (ring C atoms *cis*-/*trans*-1,4-cyclohexanedicarboxylate), 27.2 (cyclooctane) ppm. PXRD: capillary: 2θ [°] (intensity): 11.8 (34.4), 13.6 (48.8), 15.3 (65.5), 17.8 (56.5), 19.4 (23.4), 20.3 (27.7), 22.6 (15.8), 24.6 (17.0), 26.5 (36.7), 30.0 (20.4), 39.8 Pt [111] (100), 46.6 Pt [200] (31.5), 67.5 Pt [220] (27.7), 81.6 Pt [311] (38.6).

Supporting Information (see also the footnote on the first page of this article): ^{195}Pt MAS NMR of sample **1**, additional powder X-ray data of composite **6**, TEM and EDX data on composite **7** and ^{13}C MAS NMR spectroscopic data on the stability of Pt@MOF-5 under hydrogen.

Acknowledgments

The authors thank the Deutsche Forschungsgemeinschaft (DFG) for funding (Research Centre 558, "Metal-Substrate Interactions in Heterogeneous Catalysis"). Further the help of Dr. A. Trautwein, Südchemie AG, Heufeld, for ICP/AAS measurements is gratefully acknowledged. The authors would also like to thank Prof. Dr. U. Zenneck, University of Erlangen-Nürnberg, for providing [Fe(η^6-toluene)(η^4-C_4H_6)]. F. S. is grateful for a scholarship of the German DFG. S. H. is thanks the Fonds der Chemischen Industrie for a Ph.D. stipend and a fellowship by the Research School of the Ruhr University Bochum.

[1] a) S. Hermes, M.-K. Schröter, R. Schmid, L. Khodeir, M. Muhler, A. Tissler, R. W. Fischer, R. A. Fischer, *Angew. Chem. Int. Ed.* **2005**, *44*, 6237–6241; b) S. Hermes, F. Schröder, S. Amirjalayer, R. Schmid, R. A. Fischer, *J. Mater. Chem.* **2006**, *16*, 2464–2472; c) M. Sabo, A. Henschel, H. Fröde, E. Klemm, S. Kaskel, *J. Mater. Chem.* **2007**, *17*, 3827–3832; d) F. Schröder, D. Esken, M. Cokoja, M. W. E. van den Berg, O. I. Lebedev, B. Walaszek, G. Buntkowsky, H.-H. Limbach, B. Chaudret, R. A. Fischer, *J. Am. Chem. Soc.* **2008**, *130*, 6119–6130; e) S. Proch, J. Herrmannsdorfer, R. Kempe, C. Kern, A. Jess, L. Seyfarth, J. Senker, *Chem. Eur. J.* **2008**, *14*, 8204–8212; f) T. Ishida, M. Nagaoka, T. Akita, M. Haruta, *Chem. Eur. J.* **2008**, *14*, 8456–8460; g) M. Müller, S. Hermes, K. Kähler, M. W. E. van den Berg, M. Muhler, R. A. Fischer, *Chem. Mater.* **2008**, *20*, 4576–4587; h) A. Henschel, K. Gedrich, R. Kraehnert, S. Kaskel, *Chem. Commun.* **2008**, 4192–4194; i) Y. Y. Liu, J. Zhang, J. L. Zeng, H. L. Chu, F. Xu, L. X. Sun, *Chin. J. Catal.* **2008**, *29*, 655–659; j) S. Opelt, S. Turk, E. Dietzsch, A. Henschel, S. Kaskel, E. Klemm, *Catal. Commun.* **2008**, *9*, 1286–1290; k) Y. K. Hwang, D. Y. Hong, J. S. Chang, S. H. Jhung, Y. K. Seo, J. Kim, A. Vimont, M. Daturi, C. Serre, G. Ferey, *Angew. Chem. Int. Ed.* **2008**, *47*, 4144–4148; l) T. Uemura, D. Hiramatsu, K. Yoshida, S. Isoda, S. Kitagawa, *J. Am. Chem. Soc.* **2008**, *130*, 9216–9217; m) M. Müller, X. Zhang, Y. Wang, R. A. Fischer, *Chem. Commun.* **2009**, 119–121; n) D. Esken, X. Zhang, O. I. Lebedev, F. Schröder, R. A. Fischer, *J. Mater. Chem.* **2009**, *19*, 1314–1319.

[2] T. Ishida, M. Nagaoka, T. Akita, M. Haruta, *Chem. Eur. J.* **2008**, *14*, 8456–8460.

[3] S. Sun, *Adv. Mater.* **2006**, *18*, 393–403.

[4] D. Weller, M. E. Doerner, *Annu. Rev. Mater. Sci.* **2000**, *30*, 611–644.

[5] A. Moser, K. Takano, D. T. Margulies, M. Albrecht, Y. Sonobe, Y. Ikeda, S. Sun, E. E. Fullerton, *J. Phys. D: Appl. Phys.* **2002**, *35*, R157–R167.

[6] A. Giroir-Fendler, D. Richard, P. Gallezot, *J. Chem. Soc. Faraday Trans.* **1991**, *69*, 78–92.

[7] a) M. Harada, M. K. Asakura, N. Toshima, *J. Phys. Chem.* **1994**, *98*, 2653–2662; b) N. Toshima, K. Hirakawa, *Appl. Surf.*

Sci. **1997**, *121–122*, 534–537; c) N. Toshima, T. Yonezawa, *New J. Chem.* **1998**, *22*, 1179–1202.
[8] G. J. Hutchings, *Chem. Commun.* **2008**, 1148–1164.
[9] H. Vu, V. Goncales, R. Philippe, E. Lamouroux, M. Corrias, Y. Kihn, D. Plee, P. Kalck, P. Serp, *J. Catal.* **2006**, *240*, 19–22.
[10] a) T. J. Schmidt, M. Noeske, H. A. Gasteiger, R. J. Behm, P. Britz, W. Brijoux, H. Bönnemann, *Langmuir* **1997**, *13*, 2591–2595; b) W. Vogel, P. Britz, H. Bönnemann, J. Rothe, J. Horms, *J. Phys. Chem. B* **1997**, *101*, 11029–11036.
[11] a) F. Dassenoy, M.-J. Casanove, P. Lecante, C. Pan, K. Philippot, B. Chaudret, *Phys. Rev. B* **2001**, *63*, 235407 1–7; b) F. Dumestre, S. Martinez, D. Zitoun, M.-C. Fromen, M.-J. Casanove, P. Lecante, M. Respaud, A. Serres, E. Benfield, C. Amiens, B. Chaudret, *Faraday. Discuss.* **2004**, *125*, 265–278; c) C. Devaux, C. Amiens, P. Fejes, P. Renaud, M. Respaud, P. Lecante, E. Snoeck, B. Chaudret, *Nat. Mater.* **2005**, *4*, 750–753.
[12] Z. Xue, M. J. Strouse, D. K. Shuh, C. B. Knobler, H. Kaesz, R. F. Hicks, R. S. Williams, *J. Am. Chem. Soc.* **1989**, *111*, 8779–8784.
[13] R. R. Thomas, J. M. Park, *J. Electrochem. Soc.* **1989**, *136*, 1661–1666.
[14] H. Kim, H. Chun, G. H. Kim, H. S. Lee, K. Kim, *Chem. Commun.* **2006**, 2759–2761.
[15] a) L. D. Boardman, R. A. Newmark, *Magn. Res. Chem.* **1992**, *30*, 481–489; the ^{13}C NMR spectrum of [Fe(η^6-toluene)(η^4-C_4H_6)] is not known in the literature, instead comparison with ^{13}C MAS-NMR shifts of similar Fe complexes was performed; b) J. J. Schneider, U. Specht, R. Goddard, C. Krüger, J. Ensling, P. Gütlich, *Chem. Ber.* **1995**, *128*, 941–945; c) C. G. Kreiter, S. Stüber, L. Wackerle, *J. Organomet. Chem.* **1974**, *66*, C49–C52.
[16] N. H. Dryden, R. K. Kumar, E. Ou, M. Rashidi, S. Roy, P. R. Norton, R. J. Puddephatt, *Chem. Mater.* **1991**, *3*, 677–685.
[17] P. Pertici, G. Vitulli, M. Paci, L. Porri, *J. Chem. Soc., Dalton Trans.* **1980**, *10*, 1961–1964.
[18] F. Wan, H. Bönnemann, *Appl. Organomet. Chem.* **2005**, *19*, 94–97.
[19] L. Huang, H. Wang, J. Chen, Z. Wang, J. Sun, D. Zhao, Y. Yan, *Microporous Mesoporous Mater.* **2003**, *58*, 105–114.
[20] J. Hafizovic, M. Bjorgen, U. Olsbye, P. D. C. Dietzel, S. Bordiga, C. Prestipino, C. Lamberti, K. P. Lillerud, *J. Am. Chem. Soc.* **2007**, *129*, 3612–3620.
[21] A. J. Bailey, C. Lee, R. K. Feller, J. B. Orton, C. Mellot-Draznieks, B. Slater, W. T. A. Harrison, P. Simoncic, A. Navrotsky, M. C. Grossel, A. K. Cheetham, *Angew. Chem. Int. Ed.* **2008**, *47*, 8634–8637.
[22] G. Blanchard, H. Charcosset, M. Guenin, L. Tournayan, *New J. Chem.* **1981**, *5*, 85–89.
[23] a) Z. Liu, E. T. Ada, M. Shamsuzzoha, G. B. Thompson, D. E. Nikles, *Chem. Mater.* **2006**, *18*, 4946–4951; b) M. J. Hutchinson Jr., *Platinum Met. Rev.* **1972**, *16*, 88; c) T. B. Massalski (Editor-in-Chief), *Materials Information Soc.*, Materials Park, Ohio, **1990**.
[24] S. Turner, O. I. Lebedev, F. Schröder, D. Esken, R. A. Fischer, G. Van Tendeloo, *Chem. Mater.* **2008**, *20*, 5622–5627.
[25] S. Meiere, C. A. Hoover, G. L. Coon, *PCT Int. Appl.* **2003**, WO 03/106011 A2.
[26] Y. Tatsuno, T. Yoshida, S. Otsuka, *Inorg. Synth.* **1979**, *19*, 220–223.
[27] K. Itoh, H. Nagashima, T. Ohshima, N. Oshima, H. Nishiyama, *J. Organomet. Chem.* **1984**, *272*, 179–188.
[28] H. C. Clark, L. E. Manzer, *J. Organomet. Chem.* **1973**, *59*, 411–428.
[29] H. Li, M. Eddaoudi, M. O'Keeffe, O. M. Yaghi, *Nature* **1999**, *402*, 276–279.

Received: February 9, 2009
Published Online: June 22, 2009

